Journal of Integrative Neuroscience

J. Integr. Neurosci. **2025**; 24(2): 25521
https://doi.org/10.31083/JIN25521

Original Research

Application of Diffusional Kurtosis Imaging on Normal-Appearing White Matter in Cerebral Small Vessel Disease

Yue-lin Guo[1,*,†], Si-lan Chen[2,†], Hai-bing Rao[3], Ling-mei Kong[4], Wei-jia Li[4], Qi-ze Liu[4], Feng-yu Liu[1], Yu Wang[1], Wen-bin Zheng[4]

[1]Department of Radiology, Shenzhen Hospital of Integrated Traditional Chinese and Western Medicine, 518104 Shenzhen, Guangdong, China
[2]Department of Radiology, Jieyang People's Hospital, 522000 Jieyang, Guangdong, China
[3]Department of Ultrasound, Shenzhen Hospital of Integrated Traditional Chinese and Western Medicine, 518104 Shenzhen, Guangdong, China
[4]Department of Radiology, The Second Affiliated Hospital of Shantou University Medical College, 515000 Shantou, Guangdong, China
*Correspondence: lamsubmit@126.com (Yue-lin Guo)
[†]These authors contributed equally.

Academic Editor: Bettina Platt
Submitted: 12 March 2024 Revised: 26 September 2024 Accepted: 9 October 2024 Published: 27 February 2025

Abstract

Background: This study aimed to investigate the diagnostic potential of diffusional kurtosis imaging (DKI) parameters in detecting pathological alterations in the normal-appearing white matter (NAWM) associated with cerebral small vessel disease (CSVD). **Methods**: A total of 56 patients diagnosed with CSVD were enrolled, all exhibiting confirmed lacunar infarction in the corticospinal tract (CST) as verified by conventional magnetic resonance imaging. A control group of 24 healthy individuals who exhibited no discernible abnormalities on conventional magnetic resonance imaging (MRI) scans was also included. The following DKI parameters were recorded, including mean kurtosis (MK), axial kurtosis (Ka), and radial kurtosis (Kr). Regions of interest were placed at representative levels of the CST on the affected side, encompassing the pons, anterior part of the posterior limb of the internal capsule (PLIC), corona radiata, and subcortex. **Results**: Variations in MK, Ka, and Kr values in the pons, anterior part of the PLIC, corona radiata, and subcortex of the control group were observed. Notably, the MK and Kr values of the normal-appearing pons in CSVD patients were significantly elevated compared with the control group. The MK, Ka value of the normal-appearing anterior part of the PLIC was significantly higher in the CSVD group than in the control group. The Kr value of the normal-appearing corona radiata exhibited a significant elevation in CSVD patients compared with the control group. Lastly, patients with CSVD displayed lower Ka values and higher Kr values in the normal-appearing subcortex compared with the control group. **Conclusions**: DKI is an effective tool for assessing NAWM in patients with CSVD. These findings potentially offer novel insights into the prognosis of CSVD and serve as a foundational platform for future DKI studies on NAWM in other diffuse brain lesions.

Keywords: cerebral small vessel disease; corticospinal tract; normal-appearing white matter; diffusional kurtosis imaging; magnetic resonance imaging

1. Introduction

Cerebral small vessel disease (CSVD), referring to a disorder of perforating cerebral arterioles, venules, and capillaries, is one of the most common, chronic, and progressive vascular diseases that contribute to 25% of stroke cases and causes 45% of dementia [1,2]. With the accelerated aging of the world population, the incidence of CSVD has progressively increased over the years, reaching 11.5–35.7% in people aged 50–80 years [3]. The clinical manifestations of CSVD include cognitive impairment, abnormal gait, dementia, sudden stroke symptoms, and psychiatric disorders, depending on the brain regions affected and the cause of the disease [4]. Given the usually mild clinical symptoms associated with CSVD, neuroimaging has become a crucial diagnostic tool for identifying CSVD [5,6]. The main neuroimaging characteristics of CSVD consist of white matter hyperintensities or leukoaraiosis, lacunes, brain atrophy, small subcortical infarcts, enlarged perivascular spaces, and microbleeds [7,8]. Functional and structural abnormalities of brain network connections and neural pathways are vital contributors to the pathogenesis of CSVD [9]. Previous studies of CSVD have primarily focused on investigating the relationship between white matter demyelination and cognitive function [10,11]. More studies investigating brain network disruptions in CSVD patients are warranted.

The diffusional kurtosis imaging (DKI) technique in magnetic resonance imaging (MRI) has significantly improved the sensitivity and accuracy in evaluating microstructural changes in neural fibers compared to traditional diffusion tensor imaging [12–15]. A recent study used DKI to explore microstructural alternations in the cingulum of patients with CSVD and found that DKI-derived parameters could be used to characterize mild cognitive impairment in this population [16]. Another study used DKI to characterize white matter in CSVD, focusing on advanced diffusion MRI models to investigate the relation-

ship between brain microstructural alterations and declines in processing speed in CSVD patients [17]. Microstructural changes in the early stage of neuronal degeneration are usually not evident in routine MRI scans, known as normal-appearing white matter regions (NAWM) [18,19]. In this study, NAWM refers to regions where cerebral infarct lesions have led to early or mild Wallerian degeneration of their downstream nerves without manifesting any abnormalities in conventional MRI signals [20]. We hypothesized that DKI may detect the presence of NAWM in patients with CSVD, thereby providing a more accurate assessment of prognosis and treatment efficacy. Two key factors affecting the accuracy of lesion diagnosis in imaging are the homogeneity of the background and the contrast between adjacent tissues, including the lesion background and adjacent normal tissues. We believe that before studying of NAWM, it is necessary to gain a thorough understanding of the "homogeneity of the background" referring to variations in value uniformity across healthy brain regions in parametric maps, and the contrast of adjacent tissues for each DKI parameter in representative areas of normal brain tissues. A previous study compared the same parameter for different brain structures to identify its variability [21]. Brain mean kurtosis (MK), axial kurtosis (Ka), and radial kurtosis (Kr) provide distinct information in healthy white matter [22]. However, to our knowledge, no studies have specifically focused on these parameters in different brain regions.

In this study, DKI scans were performed on the corticospinal tract (CST) of patients with lacunar infarction. The CST is the largest and most anatomically distinct region of the brain and a key marker of CSVD. Using the CST as the research focus allows for more accurate localization and qualitative analysis of NAWM [23]. The homogeneity of the background and the contrast between adjacent tissues for each parameter of DKI in representative brain regions were explored, and the DKI parameters in different NAWM of the CST were analyzed. We aimed to explore the diagnostic value of DKI parameters in detecting pathological changes in the NAWM associated with CSVD.

2. Materials and Methods

2.1 Participants

In this prospective study, patients diagnosed with CSVD in the Second Affiliated Hospital of Shantou University Medical School between September 2016 and September 2023, with confirmed lacunar infarction in the CST by conventional MRI, were eligible for screening. The inclusion criteria were as follows: (1) the diagnosis of CSVD by two chief neurologists; (2) demonstration of mild neurological dysfunction [24]; (3) confirmation of non-acute lacunar cerebral infarction by conventional MRI [5]; and (4) white matter lesions observed in conventional MRI were consistent with Fazekas Grade 1 [5,25]. Patients presenting with acute cerebral infarction, cerebral hemorrhage, or infarct lesions exceeding 15 mm in diameter were excluded from the study. The raw data during and after each MRI scan were monitored and inspected. Patients with artifacts were re-scanned. Initially, 60 patients met the eligibility criteria. After the exclusion of three cases due to motion artifacts and one voluntary withdrawal, 56 patients with CSVD were finally enrolled in the CSVD group. Furthermore, we recruited 24 healthy individuals without neurologic symptoms or diseases who displayed no detectable abnormalities on conventional MRI to comprise the Control group. All participants underwent both conventional MRI and DKI scans. This study followed the Declaration of Helsinki and approved by the Research Ethics Committee of the Second Affiliated Hospital of Shantou University Medical College, and all participants or their legal guardians provided written informed consent.

2.2 Image Acquisition

All patients underwent cranial DKI and conventional MRI scans, encompassing T1-weighted images, T2-weighted images, fluid-attenuated inversion recovery, diffusion-weighted imaging, and apparent diffusion coefficient maps. These scans were conducted using a Signa EXCITE HDxT 3.0T whole-body scanner fitted in an 8-channel head coil (GE Medical System, Milwaukee, WI, USA).

The acquisition of DKI data involved a diffusion sequence employing echo planar imaging with oblique axial slices (thickness/gap: 3.0 mm/1.0 mm). All patients underwent a whole brain scan within 5 min. The acquisition parameters were configured as follows: repetition time/echo time = 500/98.6 ms; field of view = 240 $\times$ 240 mm^2; the number of excitations = 1; matrix = 128 $\times$ 128; encompassing 15 gradient encoding directions with two b values (1000 and 2000 s/mm^2) for each direction, except for b = 0.

Two radiologists at the attending level or above conducted subsequent imaging analyses, following a single-blind protocol and utilizing the DKI software of Functool 9.0 in the GE ADW4.6 workstation (GE Medical System, Rueda Minière, France). The regions of interest (ROIs) were placed at representative levels of the CST on the affected side, including pons, the anterior part of the posterior limb of the internal capsule (PLIC), corona radiata, and subcortex [5,26]. The ROI area ranges from 5 to 10 mm^2, with each ROI measured three times to determine its mean value. In case of disagreement between two radiologists regarding whether the lesion met the inclusion requirements, whether the location of the lesion corresponded to the representative level of the corticospinal tract, or which DKI parameter map most effectively displayed the lesion, a third radiologist at the deputy director level or above would conduct the analysis. A consensus would be reached through discussion.

Both MRI parameters and DKI parameters, including the MK, Ka, and Kr, were recorded. The coefficient of variation (CV) for MK, Ka, and Kr values in each brain re-

Table 1. Demographic and clinical characteristics of the CSVD and Control groups.

Item	CSVD group (n = 56)	Control group (n = 24)
Age (years; mean ± SD)	61 ± 6	60 ± 4
Male/Female (n)	33/23	9/15
NIHSS (n)		
Minor/Moderate/Severe	56/0/0	0/0/0
Risk factors for cerebral infarction		
Hypertension	35/56 (62.50%)	4/24 (16.67%)
Type 2 diabetes	15/56 (26.79%)	6/24 (25%)
Dyslipidemia	29/56 (51.79%)	10/24 (41.67%)
Coronary heart disease	4/56 (7.14%)	1/24 (4.17%)

CSVD, cerebral small vessel disease; NIHSS, National Institute of Health Stroke Scale; SD, standard deviation.

Note: NIHSS score: minor (1–4); moderate (1–15); severe (15–42).

gion was also calculated using the following formula: CV = Standard deviation/mean × 100%. Infarct foci visible in the conventional MRI were excluded.

2.3 Statistical Analysis

Data analysis was conducted utilizing SPSS 26.0 software (IBM SPSS statistics 26.0, Chicago, IL, USA). MK, Ka, and Kr values within distinct brain regions were categorized as measurement data, and their adherence to a normal distribution was evaluated through the Shapiro-Wilk test. When these data demonstrated a normal distribution, they were presented as mean ± standard deviation (SD), otherwise, they were expressed as the median with the interquartile range. The MK, Ka, and Kr of different brain regions in healthy brains of the Control group were compared using the One-way Analysis of Variance (ANOVA). The comparisons between the CSVD and Control groups were carried out Multivariate Analysis of Covariance (Hypertension, Type 2 diabetes, Dyslipidemia and Coronary heart disease as covariate), with an effect size of η^2. However, the Ka value of the normal-appearing anterior part of the PLIC did not follow a normal distribution. Multiple Regression Analysis was used to compare the CSVD and control group, with an effect size of R^2. Statistical significance was established at $p < 0.05$.

3. Results

3.1 Basic Characteristics of Both Groups

The CSVD group, comprised of 33 men and 23 women, exhibited a mean age of 61 ± 6 years, with ages ranging from 42 to 71 years. Conversely, the Control group, consisting of 9 men and 15 women, had a mean age of 60 ± 4 years, spanning from 52 to 68 years. Notably, there were no statistically significant differences in age ($t = 0.16$) or gender ($\chi^2 = 3.09$) observed between the two groups (both $p > 0.05$). In addition, all CSVD patients exhibited scores indicative of minor strokes on the National Institute of Health Stroke Scale (NIHSS). Risk factors for cerebral infarction include Hypertension, Type 2 diabetes, Dyslipidemia, Coronary heart disease (Table 1).

3.2 The DKI Parameters of Different Brain Regions in Healthy Brains of the Control Group

The MK, Ka, and Kr values of the pons, anterior part of the PLIC, corona radiata, and subcortex in healthy brains of the Control group were significantly different (all $p < 0.01$; the F values were 200.21, 80.46, 109.77, and 92.59, respectively). The CV for MK, Ka, and Kr in each brain region was also significantly different (Fig. 1).

3.3 Characteristics of Lacunar Infarct Foci in Different Brain Regions of the CST on DKI

According to the conventional MRI, substantial changes in the Ka maps were observed when the non-acute stage lacunar infarction foci were situated in the anterior part of the PLIC (positive rate: 62.5%). Substantial alterations in the Kr maps were found when the lesion was in the subcortex (positive rate: 64.29%). Lesions in the pons and corona radiata were most prominently displayed in the MK maps (positive rate: 48.21% and 39.29%, respectively) (Fig. 2).

3.4 The DKI Parameters of Different Brain Regions of the CSVD and Control Groups

The MK, Ka, and Kr values of the normal-appearing pons of the CSVD group were elevated compared with the Control group, with statistical significance observed in the MK and Kr values ($F_{MK} = 23.90$, $P_{MK} < 0.01$, $F_{Kr} = 159.56$, $P_{Kr} < 0.01$) (η^2 for MK and Ka were 0.24 and 0.68, respectively). The MK, Ka value of the normal-appearing anterior part of the PLIC was significantly higher in the CSVD group than in healthy subjects ($F_{MK} = 645.38$, $P_{MK} < 0.01$, $\eta^2 = 0.90$, $F_{Ka} = 2.55$, $P_{Ka} = 0.04$, $R^2 = 0.15$). Additionally, the Kr value of the normal-appearing corona radiata of the CSVD group exhibited a significant elevation compared with the Control group ($F_{Kr} = 9.39$, $P_{Kr} < 0.01$, $\eta^2 = 0.11$). Patients with CSVD also showed lower Ka values and higher MK and Kr values in the normal-appearing subcortex compared with healthy individuals ($F_{Ka} = 11.31$, $P_{Ka} < 0.01$, $F_{Kr} = 6.68$, $P_{Kr} = 0.01$), (η^2 for Ka and Kr were 0.13 and 0.08, respectively) (Fig. 3).

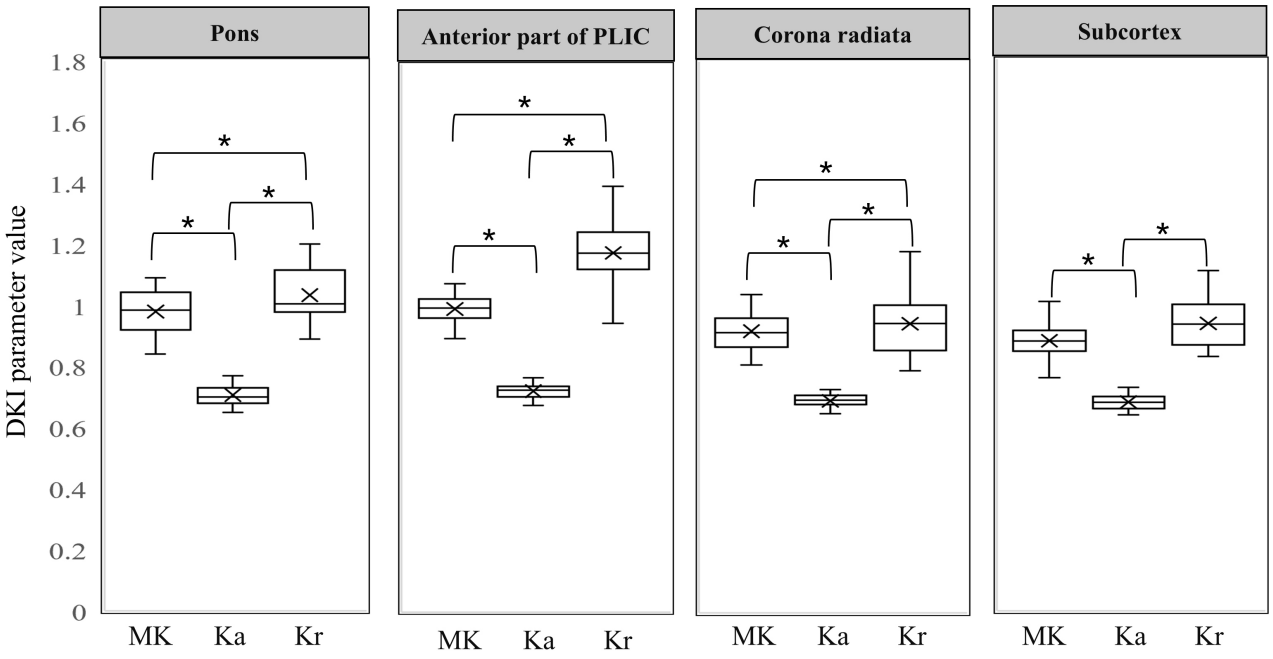

Fig. 1. DKI parameters value of different brain regions in healthy brains of the control group. DKI, diffusional kurtosis imaging; PLIC, posterior limb of the internal capsule. * indicates statistical significance among different DKI parameters ($p < 0.01$). Note: The variations of different DKI parameter values in healthy brains reflect variations in value uniformity across healthy brain regions in parametric maps. MK, mean kurtosis; Ka, axial kurtosis; Kr, radial kurtosis.

4. Discussion

Nodular lesions within the brain, which lead to a cascade of neuronal dysfunction or damage, contribute significantly to the pathogenesis of CSVD [27]. Previous investigations have demonstrated that conventional mean diffusivity maps show increased values in white matter lesions but not in NAWM [12]. Brain abnormalities induced by cerebral infarction may be undetected in routine MRI sequences, such as T1 and T2 weighted images, fluid-attenuated inversion recovery, and conventional diffusion-weighted MRI sequences, including diffusion-weighted imaging, apparent diffusion coefficient maps, and diffusion tensor imaging [28]. However, these abnormalities can be effectively identified using DKI [29–31]. In this study, we demonstrated the presence of NAWM in cases of lacunar infarction within the CST and proved that DKI is a valuable tool for detecting microstructural alterations within these regions.

NAWM refers to regions where cerebral infarct lesions have led to early or mild Wallerian degeneration of their downstream nerves without manifesting any abnormalities in conventional MRI signals [20]. Signal heterogeneity in MK, Ka, and Kr maps plays a pivotal role in assessing NAWM in cases of CSVD [12,13]. Our initial findings revealed significant differences among MK, Ka, and Kr in each brain region of the Control group (all $p < 0.05$). The CV for MK, Ka, and Kr in each brain region was also significantly different (Fig. 1), suggesting variations in value uniformity across healthy brain regions in parametric maps. Furthermore, the diagnostic efficacy of MK, Ka, and Kr maps in identifying lacunar infarcts in different brain regions showed variability (Fig. 2).

When lacunar infarction foci were localized in the anterior part of the PLIC, noticeable changes were observed in the Ka maps. Similarly, significant alterations were detected in the Kr maps when the lesion was situated in the subcortex. Lesions within the pons and corona radiata were most prominently depicted in the MK maps. These findings are consistent with previous reports [12,13]. A homogeneous background and the contrast between adjacent tissues (including contrast between lesion-background and contrast between adjacent normal tissue) in the DKI maps are the two pivotal factors for the comprehensive analysis of NAWM in cases of CSVD.

The differences (anisotropy) of Brownian motion of water molecules in brain tissues, which varies in different directions, are closely related to the direction of nerve fiber routing [13]. The values of DKI parameters (i.e., MK, Ka, and Kr) differ in different brain regions. Ka reflects the Brownian motion of water molecules in the direction of the axons. Kr represents the influence of the hydrophobicity of the axonal myelin sheath on the Brownian motion of water molecules. MK indicates the complexity of the local microstructure. These DKI parameters have been extensively discussed in previous DKI studies, and our results are consistent with these findings. The pons represent a re-

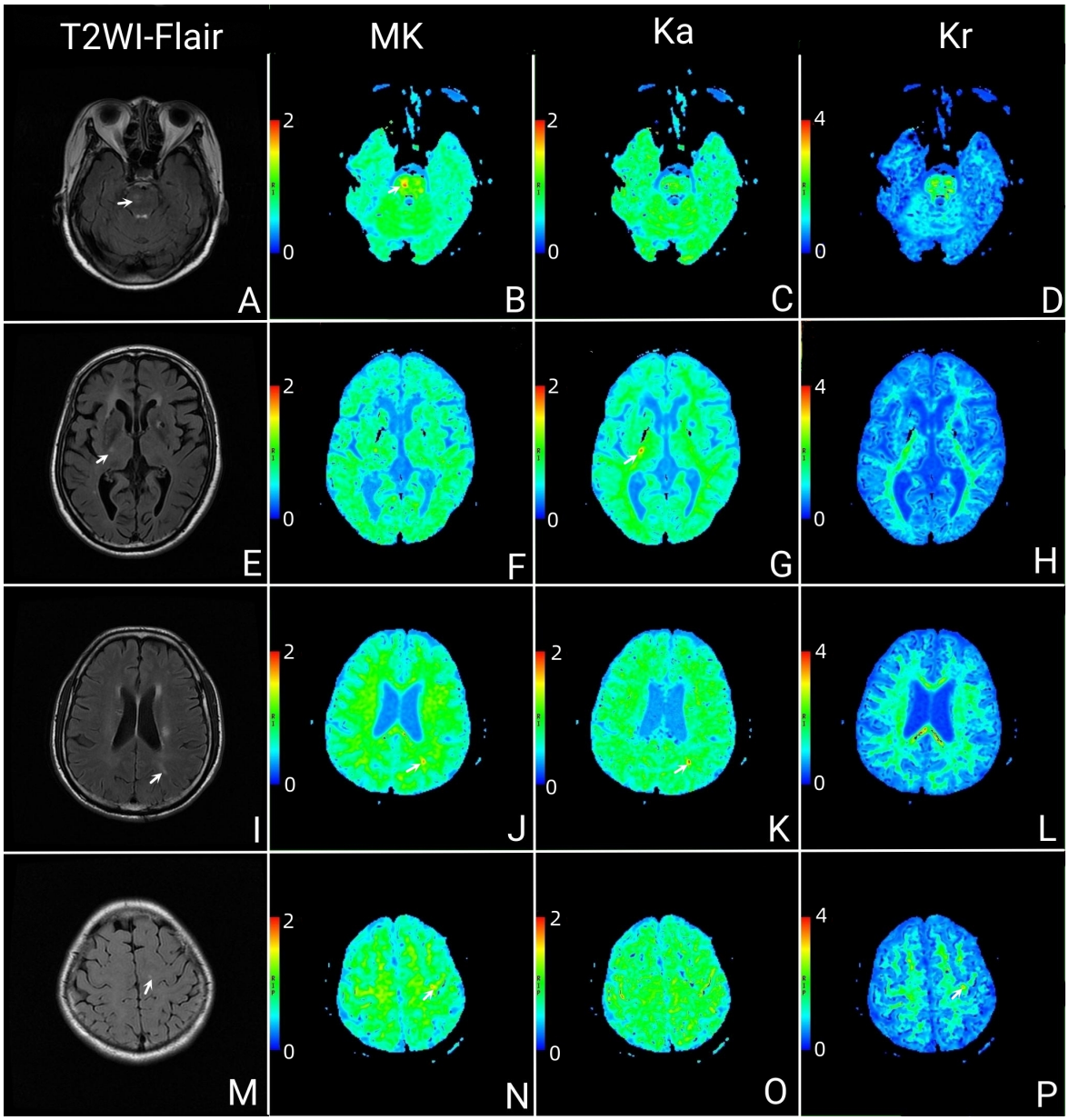

Fig. 2. Characteristics of lacunar infarct foci in different brain regions of the CST on DKI. The lesion within the pons showed high signal on Flair (A, white arrow), and it was most prominently depicted in the MK maps (B, white arrow). Lesions within the pons were barely visible in the Ka maps (C) and Kr maps (D). The lesion within the PLIC showed high signal on Flair (E, white arrow), and it was most prominently depicted in the Ka maps (G, white arrow). Lesions within the PLIC were barely visible in the MK maps (F) and Kr maps (H). The lesion within the corona radiata showed high signal on Flair (I, white arrow). Lesion within the corona radiata was most prominently depicted in the MK maps (J, white arrow), but it was unclear displayed in the Ka maps (K, white arrow) and invisible in the Kr maps (L). The lesion within the subcortex showed high signal on Flair (M, white arrow). Lesion within the subcortex was most prominently depicted in the Kr maps (P, white arrow), but it was unclear displayed in the MK maps (N, white arrow) and invisible in the Ka maps (O). T2WI, T2-weighted images; Flair, fluid-attenuated inversion recovery; CST, corticospinal tract; DKI, diffusional kurtosis imaging. Note: (1) Diagnostic efficacy: The lesions were first found with the naked eye following a single-blind protocol, and the differences between the lesions and the mirrored normal brain areas were measured at the workstation. The DKI parameter map with the greatest difference between the lesion and the mirror normal brain area is defined as the one with the highest diagnostic efficacy (white arrow). (2) The diagnostic efficacy of MK, Ka, and Kr maps in identifying lacunar infarcts in different brain regions displayed variability. (3) The different rows of panels related to different patients.

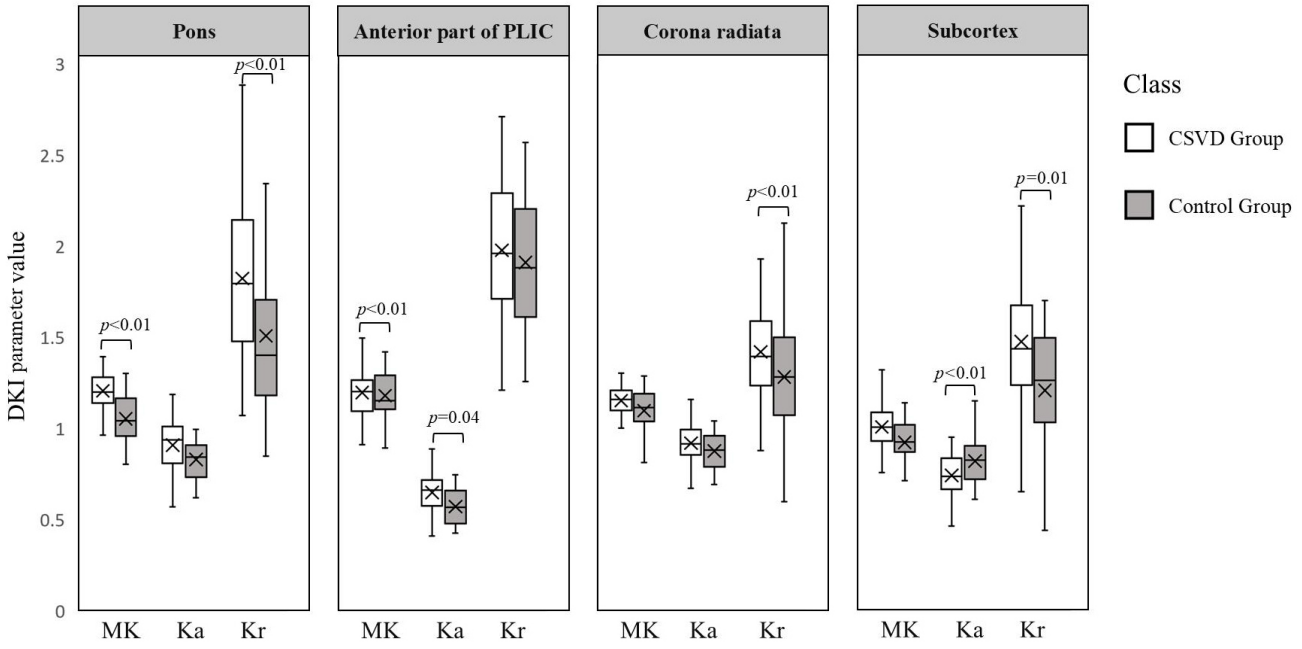

Fig. 3. The MK, Ka and Kr values of different brain regions of the CSVD and Control groups. PLIC, posterior limb of the internal capsule; CSVD, cerebral small vessel disease. Note: The differences (anisotropy) of Brownian motion of water molecules in brain tissues in various directions are closely related to the direction of nerve fiber routing.

gion where nerve fibers converge with relatively consistent directional alignment, displaying relatively high anisotropy [13]. In the case of CSVD patients, the MK, Ka, and Kr values of the pons were elevated compared to the Control group, with statistically significant differences observed in the MK and Kr values. In the anterior part of the PLIC, nerve fibers exhibit the highest level of anisotropy, indicating directional consistency [13]. Due to the elevated background signal in this region, the Ka value showed a significant increase in CSVD patients compared to healthy subjects. In contrast, the corona radiata primarily consists of divergent nerve fibers characterized by low directional consistency and anisotropy [13]. In this case, the Kr value of the corona radiata was significantly higher in the CSVD group than in the Control group. Lastly, the subcortex primarily comprises arcuate fibers, exhibiting the lowest directional consistency and anisotropy compared to the pons, the anterior part of the PLIC, and corona radiata. CSVD patients displayed lower Ka and higher Kr values in the subcortex compared to healthy individuals. These discrepancies in the changes of Ka, MK, and Kr values may suggest compensatory alterations in proximal axons due to injury. Previous animal studies have indicated aberrant expression of neuro-related antibodies, such as neurofilament-200 and glial fibrillary acidic protein, at different stages of cerebral infarction [32–34]. Further studies are required to ascertain whether NAWM in patients with CSVD is linked to compensatory changes in proximal nerve fibers.

The current study is limited by a relatively small sample size. Future investigations are needed to enhance statistical power by enlarging the sample size, allowing for a more comprehensive analysis of subgroups within the case cohort. Additionally, longitudinal follow-up studies on a patient cohort are warranted to provide insights into the dynamic progression of CSVD. In addition, using 15 gradient directions for DKI scanning is insufficient, as it may compromise the accuracy and precision of the estimates. Finally, to enhance the understanding of the microstructural changes in minor vessel diseases, it is necessary to improve the establishment of diffusion models, such as the reproducibility of diffusion metrics.

5. Conclusions

DKI is an effective method for evaluating NAWM in patients with CSVD. We recommend establishing evaluation criteria based on the anisotropy and background signal of NAWM. Our findings may offer new perspectives for the prognostic assessment of CSVD and serve as a basis for DKI studies of NAWM in other diffuse brain lesions, such as multiple sclerosis and neuromyelitis optica.

Availability of Data and Materials

The data sets generated and/or analyzed during the current study are not publicly available due to their containing information that could compromise the privacy of research participants, and some of which will also be used for further research.

Author Contributions

YG, SC, HR, WZ and LK conceived and designed the experiments. YG, SC, HR, WL, QL, FL and YW performed the experiments. SC, LK, WL, FL and YW analyzed the data. HR, LK, WL, QL, FL and YW prepared the figures and tables. SC wrote the manuscript. YG and WZ revised it critically for important content. All authors contributed to editorial changes in the manuscript. All authors read and approved the final manuscript. All authors have participated sufficiently in the work and agreed to be accountable for all aspects of the work.

Ethics Approval and Consent to Participate

This study was follow the Declaration of Helsinki and approved by the Research Ethics Committee of the Second Affiliated Hospital of Shantou University Medical College, and all participants or their legal guardians furnished written informed consent (approval number: 2016-29).

Acknowledgment

Not applicable.

Funding

This research was funded by the Natural Science Foundation of Shenzhen (JCYJ20190808095403639), Shenzhen Bao'an TCM Development Foundation (2022KJCX-ZJZL-4) and the Sanming Project of Medicine in Shenzhen (AZZYSM 202106006).

Conflict of Interest

The authors declare no conflict of interest.

References

[1] Litak J, Mazurek M, Kulesza B, Szmygin P, Litak J, Kamieniak P, *et al*. Cerebral Small Vessel Disease. International Journal of Molecular Sciences. 2020; 21: 9729.

[2] Cannistraro RJ, Badi M, Eidelman BH, Dickson DW, Middlebrooks EH, Meschia JF. CNS small vessel disease: A clinical review. Neurology. 2019; 92: 1146–1156.

[3] Mu R, Qin X, Guo Z, Meng Z, Liu F, Zhuang Z, *et al*. Prevalence and Consequences of Cerebral Small Vessel Diseases: A Cross-Sectional Study Based on Community People Plotted Against 5-Year Age Strata. Neuropsychiatric Disease and Treatment. 2022; 18: 499–512.

[4] Li Q, Yang Y, Reis C, Tao T, Li W, Li X, *et al*. Cerebral Small Vessel Disease. Cell Transplantation. 2018; 27: 1711–1722.

[5] Duering M, Biessels GJ, Brodtmann A, Chen C, Cordonnier C, de Leeuw FE, *et al*. Neuroimaging standards for research into small vessel disease-advances since 2013. The Lancet. Neurology. 2023; 22: 602–618.

[6] Man S, Chen S, Xu Z, Zhang H, Cao Z. Increased Extracellular Water in Normal-Appearing White Matter in Patients with Cerebral Small Vessel Disease. Journal of Integrative Neuroscience. 2024; 23: 46.

[7] Caunca MR, De Leon-Benedetti A, Latour L, Leigh R, Wright CB. Neuroimaging of Cerebral Small Vessel Disease and Age-Related Cognitive Changes. Frontiers in Aging Neuroscience. 2019; 11: 145.

[8] Inoue Y, Shue F, Bu G, Kanekiyo T. Pathophysiology and probable etiology of cerebral small vessel disease in vascular dementia and Alzheimer's disease. Molecular Neurodegeneration. 2023; 18: 46.

[9] Gu Y, Zhao P, Feng W, Xia X, Tian X, Yan Y, *et al*. Structural brain network measures in elderly patients with cerebral small vessel disease and depressive symptoms. BMC Geriatrics. 2022; 22: 568.

[10] Brandhofe A, Stratmann C, Schüre JR, Pilatus U, Hattingen E, Deichmann R, *et al*. T_2 relaxation time of the normal-appearing white matter is related to the cognitive status in cerebral small vessel disease. Journal of Cerebral Blood Flow and Metabolism: Official Journal of the International Society of Cerebral Blood Flow and Metabolism. 2021; 41: 1767–1777.

[11] Dao E, Tam R, Hsiung GYR, Ten Brinke L, Crockett R, Barha CK, *et al*. Exploring the Contribution of Myelin Content in Normal Appearing White Matter to Cognitive Outcomes in Cerebral Small Vessel Disease. Journal of Alzheimer's Disease: JAD. 2021; 80: 91–101.

[12] Guo YL, Zhang ZP, Zhang GS, Kong LM, Rao HB, Chen W, *et al*. Evaluation of mean diffusion and kurtosis MRI mismatch in subacute ischemic stroke: Comparison with NIHSS score. Brain Research. 2016; 1644: 231–239.

[13] Guo YL, Li SJ, Zhang ZP, Shen ZW, Zhang GS, Yan G, *et al*. Parameters of diffusional kurtosis imaging for the diagnosis of acute cerebral infarction in different brain regions. Experimental and Therapeutic Medicine. 2016; 12: 933–938.

[14] Jensen JH, Helpern JA, Ramani A, Lu H, Kaczynski K. Diffusional kurtosis imaging: the quantification of non-gaussian water diffusion by means of magnetic resonance imaging. Magnetic Resonance in Medicine. 2005; 53: 1432–1440.

[15] Tabesh A, Jensen JH, Ardekani BA, Helpern JA. Estimation of tensors and tensor-derived measures in diffusional kurtosis imaging. Magnetic Resonance in Medicine. 2011; 65: 823–836.

[16] Liu Y, Liu D, Liu M, Li K, Shi Q, Wang C, *et al*. The microstructural abnormalities of cingulum was related to patients with mild cognitive impairment: a diffusion kurtosis imaging study. Neurological Sciences: Official Journal of the Italian Neurological Society and of the Italian Society of Clinical Neurophysiology. 2023; 44: 171–180.

[17] Konieczny MJ, Dewenter A, Ter Telgte A, Gesierich B, Wiegertjes K, Finsterwalder S, *et al*. Multi-shell Diffusion MRI Models for White Matter Characterization in Cerebral Small Vessel Disease. Neurology. 2021; 96: e698–e708.

[18] Khan AR, Chuhutin A, Wiborg O, Kroenke CD, Nyengaard JR, Hansen B, *et al*. Biophysical modeling of high field diffusion MRI demonstrates micro-structural aberration in chronic mild stress rat brain. NeuroImage. 2016; 142: 421–430.

[19] Shepherd TM, Kirov II, Charlson E, Bruno M, Babb J, Sodickson DK, *et al*. New rapid, accurate T_2 quantification detects pathology in normal-appearing brain regions of relapsing-remitting MS patients. NeuroImage. Clinical. 2017; 14: 363–370.

[20] Puig J, Pedraza S, Blasco G, Daunis-I-Estadella J, Prats A, Prados F, *et al*. Wallerian degeneration in the corticospinal tract evaluated by diffusion tensor imaging correlates with motor deficit 30 days after middle cerebral artery ischemic stroke. AJNR. American Journal of Neuroradiology. 2010; 31: 1324–1330.

[21] Chen Y, Zhao X, Ni H, Feng J, Ding H, Qi H, *et al*. Parametric mapping of brain tissues from diffusion kurtosis tensor. Computational and Mathematical Methods in Medicine. 2012; 2012: 820847.

[22] Wu EX, Cheung MM. MR diffusion kurtosis imaging for neural tissue characterization. NMR in Biomedicine. 2010; 23: 836–848.

[23] Rudilosso S, Rodríguez-Vázquez A, Urra X, Arboix A. The Potential Impact of Neuroimaging and Translational Research on the Clinical Management of Lacunar Stroke. International Journal of Molecular Sciences. 2022; 23: 1497.
[24] Olivato S, Nizzoli S, Cavazzuti M, Casoni F, Nichelli PF, Zini A. e-NIHSS: an Expanded National Institutes of Health Stroke Scale Weighted for Anterior and Posterior Circulation Strokes. Journal of Stroke and Cerebrovascular Diseases: the Official Journal of National Stroke Association. 2016; 25: 2953–2957.
[25] Fazekas F, Chawluk JB, Alavi A, Hurtig HI, Zimmerman RA. MR signal abnormalities at 1.5 T in Alzheimer's dementia and normal aging. AJR. American Journal of Roentgenology. 1987; 149: 351–356.
[26] Mastropietro A, Rizzo G, Fontana L, Figini M, Bernardini B, Straffi L, *et al*. Microstructural characterization of corticospinal tract in subacute and chronic stroke patients with distal lesions by means of advanced diffusion MRI. Neuroradiology. 2019; 61: 1033–1045.
[27] Zhang L, Biessels GJ, Hilal S, Chong JSX, Liu S, Shim HY, *et al*. Cerebral microinfarcts affect brain structural network topology in cognitively impaired patients. Journal of Cerebral Blood Flow & Metabolism. 2021; 41: 105–115.
[28] Gons RAR, de Laat KF, van Norden AGW, van Oudheusden LJB, van Uden IWM, Norris DG, *et al*. Hypertension and cerebral diffusion tensor imaging in small vessel disease. Stroke. 2010; 41: 2801–2806.
[29] Zhu LH, Zhang ZP, Wang FN, Cheng QH, Guo G. Diffusion kurtosis imaging of microstructural changes in brain tissue affected by acute ischemic stroke in different locations. Neural Regeneration Research. 2019; 14: 272–279.
[30] Yin J, Sun H, Wang Z, Ni H, Shen W, Sun PZ. Diffusion Kurtosis Imaging of Acute Infarction: Comparison with Routine Diffusion and Follow-up MR Imaging. Radiology. 2018; 287: 651–657.
[31] Fan L, Ibrahim FEEM, Chu X, Fu Y, Yan H, Wu Z, *et al*. Altered Microstructural Changes Detected by Diffusion Kurtosis Imaging in Patients With Cognitive Impairment After Acute Cerebral Infarction. Frontiers in Neurology. 2022; 13: 802357.
[32] Liang W, Zhang W, Zhao S, Li Q, Liang H, Ceng R. Altered expression of neurofilament 200 and amyloid-β peptide (1-40) in a rat model of chronic cerebral hypoperfusion. Neurological Sciences. 2015; 36: 707–712.
[33] Lee J, Kim JG, Hong S, Kim YS, Ahn S, Kim R, *et al*. Longitudinal intravital imaging of cerebral microinfarction reveals a dynamic astrocyte reaction leading to glial scar formation. Glia. 2022; 70: 975–988.
[34] Chen D, Hou S, Chen Y. Effects of alteplase on neurological deficits and expression of GFAP and GAP-43 in brain tissue of rats with acute cerebral infarction. American Journal of Translational Research. 2021; 13: 10608–10616.